

Static magnetic solution in magnetic composites with arbitrary susceptibility inhomogeneity and anisotropy

J. J. Wang, Y. Song, X. Q. Ma, Long-Qing Chen, and Ce-Wen Nan

Citation: [Journal of Applied Physics](#) **117**, 043907 (2015); doi: 10.1063/1.4906567

View online: <http://dx.doi.org/10.1063/1.4906567>

View Table of Contents: <http://scitation.aip.org/content/aip/journal/jap/117/4?ver=pdfcov>

Published by the [AIP Publishing](#)

Articles you may be interested in

[Nonlinear susceptibility and dynamic hysteresis loops of magnetic nanoparticles with biaxial anisotropy](#)

J. Appl. Phys. **113**, 053903 (2013); 10.1063/1.4789848

[Static and high frequency magnetic and dielectric properties of ferrite-ferroelectric composite materials](#)

J. Appl. Phys. **100**, 084905 (2006); 10.1063/1.2357990

[Composite-anisotropy amorphous magnetic materials for high-frequency devices](#)

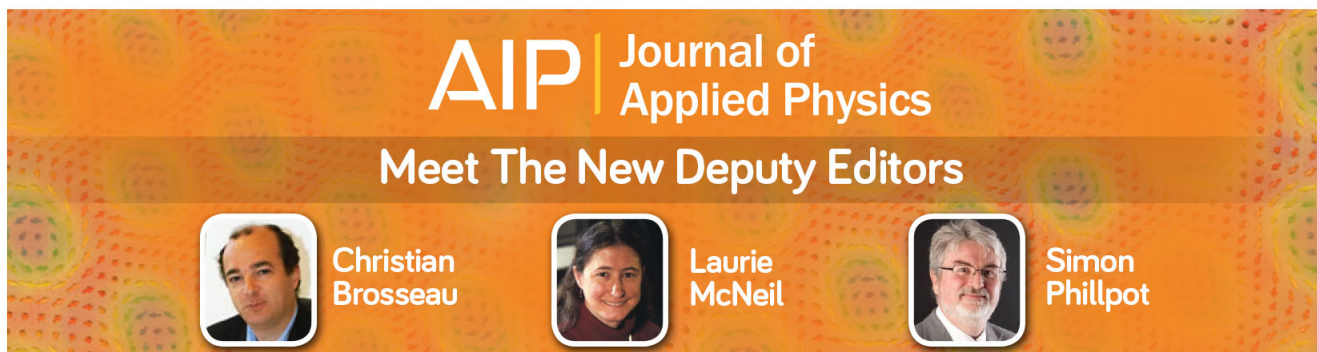
J. Appl. Phys. **97**, 10F911 (2005); 10.1063/1.1858111

[Effective-susceptibility tensor for a composite with ferromagnetic inclusions: Enhancement of effective-media theory and alternative ferromagnetic approach](#)

J. Appl. Phys. **95**, 6289 (2004); 10.1063/1.1713042

[Exchange anisotropy determined by magnetic field dependence of ac susceptibility](#)


J. Appl. Phys. **94**, 4544 (2003); 10.1063/1.1605816

A banner for the Journal of Applied Physics featuring the AIP logo and the text 'Meet The New Deputy Editors'. Below the text are three circular portraits of the new deputy editors: Christian Brosseau, Laurie McNeil, and Simon Phillpot.

AIP | Journal of Applied Physics

Meet The New Deputy Editors

 Christian Brosseau

 Laurie McNeil

 Simon Phillpot

Static magnetic solution in magnetic composites with arbitrary susceptibility inhomogeneity and anisotropy

J. J. Wang,^{1,2} Y. Song,³ X. Q. Ma,⁴ Long-Qing Chen,^{1,2} and Ce-Wen Nan¹

¹*School of Materials Science and Engineering, State Key Lab of New Ceramics and Fine Processing, Tsinghua University, Beijing 100084, China*

²*Department of Materials Science and Engineering, The Pennsylvania State University, University Park, Pennsylvania 16802, USA*

³*Shenzhen Key Lab of Electrochemical Storage Devices, Research Institute of Tsinghua University in Shenzhen, Shenzhen 518057, China*

⁴*Department of Physics, University of Science and Technology Beijing, Beijing 100083, China*

(Received 28 October 2014; accepted 14 January 2015; published online 26 January 2015)

The static magnetic solutions in magnetic composites with arbitrary susceptibility inhomogeneity and anisotropy are accurately computed using an efficient numerical algorithm based on a proposed Fourier spectral iterative perturbation method for 3-dimensional systems. An advantage of this method is that the interphase boundary conditions are automatically considered without explicitly tracking interphase interfaces in the composites. This method can be conveniently implemented in phase-field modeling of microstructure evolution in systems with inhomogeneous susceptibility as well as inhomogeneous spontaneous magnetization distributions. Based on the proposed method, the effects of microstructures including the susceptibility mismatch between the inclusions and matrix, inclusions volume fraction, and inclusions arrangement on the effective susceptibility and local static magnetic field distribution of the composite are investigated. It is found that the interactions among the inclusions embedded in the matrix play critical roles in determining the composite properties. © 2015 AIP Publishing LLC.

[<http://dx.doi.org/10.1063/1.4906567>]

I. INTRODUCTION

Composite materials are becoming more competitive because novel functionalities and enhanced properties can be generated by mixing the different pure (uniform, homogeneous, and single-phase) materials.^{1–5} Among the various composite materials, magnetic particle-filled composites can be utilized for making smart materials.^{6,7} Composite materials are normally characterized by effective coefficients, and, in magnetic composites, the effective magnetic susceptibility is of interest. The effective magnetic susceptibility depends not only on the constituent materials but also on the microstructures of the magnetic composites. For composites with arbitrary structure, the theoretical determination of the effective magnetic susceptibility is very difficult and is possible only in certain approximations. For instances, Maxwell-Garnett's (MG) model can be used to calculate the effective magnetic susceptibility of magnetic composites containing randomly dispersed spherical particles,^{8,9} but it always underestimates the effective magnetic susceptibility because this model totally neglects the interaction between particles, and thus, it will introduce large error especially when the volume fraction of the inclusion particles is high. In order to take account into the local interactions between particles, Bruggeman and Hanai *et al.* proposed an integrate equation (namely, the famous Bruggeman-Hanai (BH) equation), which showed good agreement between the theoretical prediction and experimental results.^{10–12} Based on the Bruggeman-Hanai equation, Looyenga also proposed another variation equation by assuming that the heterogeneous constitute is composed by two similar “fictitious phases.”¹³

Additionally, Hashin and Shtrikman obtained the upper and lower bounds of the effective magnetic susceptibility for magnetic composite using a variational approach.¹⁴ By considering more rigorous approximation based on the Maxwell-Garnett's model, Meredith and Tobias proposed a modified higher order equation to calculate the effective coefficients of the composite.¹⁵ By employing the Green function with corresponding boundary conditions, Fu *et al.* derived an explicit effective permittivity of dielectric composites containing spherical particles from an analytical approach.¹⁶ With the extension of Eshelby's equivalent inclusion method, Pittini-Yamada *et al.* formulated the effective magnetic susceptibility of a three-phase hybrid soft magnetic composite.¹⁷ Besides limited by the applicable conditions, the above-mentioned approximations are only focused on the estimation of the effective coefficients but unavailable to obtain the local static magnetic field distribution. Therefore, it is quite necessary to develop a more efficient algorithm which can be used to obtain both the effective magnetic susceptibility and local field distribution for magnetic composites with arbitrary magnetic susceptibility inhomogeneity and anisotropy.

Based on phase-field model, Wang *et al.* used the magnetization or polarization as the order parameter in the Ginzburg-Landau kinetic equation to minimize the total magnetic or electric free energy of the magnetic or dielectric composites; thus, the electrostatic or static magnetic equilibrium equation can be satisfied automatically when the order parameter is evolved to be quasi-stable.¹⁸ Then, the effective magnetic susceptibility and local field distribution can be

calculated from the magnetization/polarization response under externally applied magnetic/electric fields. In fact, this method was already used by Wang *et al.* to solve the mechanical equilibrium equation of elastic composites with elastic inhomogeneity and anisotropy in their earlier works.^{19,20} In our previous work, we proved that the mechanical equilibrium equation of composites with arbitrary elastic inhomogeneity and anisotropy can also be solved more efficiently by other numerical algorithms based on the so-called spectral iterative perturbation method (SPM).²¹ This SPM has been successfully used in solving the mechanical equilibrium equation in various elastically inhomogeneous systems^{22–25} and electrostatic equilibrium equation in ferroelectric-nanoparticle systems.²⁶ Moreover, the physical laws in dielectric and magnetic composites are very similar. Therefore, the SPM should be a good and efficient tool for studying the magnetic composites. In this paper, we will derive the SPM in detail for magnetic composites and present its accuracy and efficiency for calculating the effective magnetic susceptibility and local static magnetic field distribution.

The rest of this paper is organized as follows. In Sec. II, we use the SPM to solve the static magnetic equilibrium equation in magnetic composites with arbitrary magnetic susceptibility inhomogeneity and anisotropy. In Sec. III, we first take two special examples to compare the numerical result of the proposed model with the results obtained from the analytical expression; then we calculate some properties of a two-phase composite by comparing the numerical result with other theoretical approximation to numerically illustrate the validity of the proposed model. Finally, the paper ends with a short summary in Sec. IV.

II. SOLUTION OF THE STATIC MAGNETIC EQUILIBRIUM EQUATION BY SPM

In this section, we show a general description of an arbitrary magnetic composite system and then solve the static magnetic equilibrium equations using the Fourier spectral iterative perturbation scheme. An arbitrary magnetic composite in this work is described by the spatial position-dependent magnetic susceptibility $\chi^m(\mathbf{r})$, whose dependency on the magnetic field relies on the constitute materials. Note that besides the spatial position, the magnetic susceptibility $\chi^m(\mathbf{r})$ in the proposed model also can be functions of externally applied magnetic field and frequency, but in this work, all the calculations are done with assumption that $\chi^m(\mathbf{r})$ is only dependent on the spatial position, i.e., each constitution of the composite has a constant magnetic susceptibility which corresponds to the saturated part of the magnetization curve. The field and spatially position-dependent local magnetization $\mathbf{M}(\mathbf{r}, \mathbf{H})$ under a magnetic field in the magnetic composite may be written as

$$\mathbf{M}(\mathbf{r}, \mathbf{H}) = \mathbf{M}^S(\mathbf{r}) + \chi^m(\mathbf{r})\mathbf{H}(\mathbf{r}), \quad (1)$$

where $\mathbf{M}^S(\mathbf{r})$ is called as the spontaneous magnetization, which is nonzero in ferromagnetics or ferrimagnetics and zero in paramagnetics or antiferromagnetics, and the total magnetic field $\mathbf{H}(\mathbf{r})$ originates from the external magnetic

field \mathbf{H}^{ext} induced by the externally fixed current or magnet and the demagnetization field $\mathbf{H}^d(\mathbf{r})$, i.e.,

$$\mathbf{H}(\mathbf{r}) = \mathbf{H}^{\text{ext}} + \mathbf{H}^d(\mathbf{r}). \quad (2)$$

From the analysis above, the magnetic induction $\mathbf{B}(\mathbf{r}, \mathbf{H})$ in the composite can be written as

$$\begin{aligned} \mathbf{B}(\mathbf{r}, \mathbf{H}) &= \mu_0(\mathbf{H}(\mathbf{r}) + \mathbf{M}(\mathbf{r}, \mathbf{H})), \\ &= \mu_0(\mathbf{H}(\mathbf{r}) + \mathbf{M}^S(\mathbf{r}) + \chi^m(\mathbf{r})\mathbf{H}(\mathbf{r})), \\ &= \mu_0(\boldsymbol{\mu}(\mathbf{r})\mathbf{H}(\mathbf{r}) + \mathbf{M}^S(\mathbf{r})), \end{aligned} \quad (3)$$

where $\boldsymbol{\mu}(\mathbf{r}) = \boldsymbol{\delta} + \chi^m(\mathbf{r})$ is named relative permeability and $\boldsymbol{\delta}$ is the Dirac delta function.

Rewriting the physical variables with bold font in Eq. (3) in terms of components of vectors and tensors using Einstein notation, the magnetic induction is as follows:

$$B_i(\mathbf{r}, \mathbf{H}) = \mu_0(\mu_{ij}(\mathbf{r})H_j(\mathbf{r}) + M_i^S(\mathbf{r})). \quad (4)$$

The Gauss's law for magnetism requires that the divergence of the magnetic induction equals to zero, i.e.,

$$\frac{\partial B_i(\mathbf{r}, \mathbf{H})}{\partial x_i} = \frac{\partial [\mu_0(\mu_{ij}(\mathbf{r})H_j(\mathbf{r}) + M_i^S(\mathbf{r}))]}{\partial x_i} = 0. \quad (5)$$

We introduce another physical variable $\varphi_m(\mathbf{r})$ which is related to the demagnetization field by

$$H_j^d(\mathbf{r}) = -\nabla_j \varphi_m(\mathbf{r}), \quad (6)$$

and here, we name it the demagnetization potential. Substituting Eqs. (2) and (6) into Eq. (5), we have

$$\frac{\partial \left[\mu_{ij}(\mathbf{r}) \left(H_j^{\text{ext}} - \frac{\partial \varphi_m(\mathbf{r})}{\partial x_j} \right) + M_i^S(\mathbf{r}) \right]}{\partial x_i} = 0. \quad (7)$$

The position-dependent relative permeability can be written in sum of homogeneous reference μ_{ij}^0 and inhomogeneous perturbation $\Delta\mu_{ij}(\mathbf{r})$, i.e.,

$$\mu_{ij}(\mathbf{r}) = \mu_{ij}^0 + \Delta\mu_{ij}(\mathbf{r}). \quad (8)$$

Substituting Eq. (8) into Eq. (7) and rearranging it, we can obtain

$$\mu_{ij}^0 \frac{\partial^2 \varphi_m(\mathbf{r})}{\partial x_i \partial x_j} = \frac{\partial}{\partial x_i} \left[\Delta\mu_{ij}(\mathbf{r}) \left(H_j^{\text{ext}} - \frac{\partial \varphi_m(\mathbf{r})}{\partial x_j} \right) + M_i^S(\mathbf{r}) \right]. \quad (9)$$

Equation (9) is the key static magnetic equilibrium equations for an magnetic composite system. With the assumption that Eq. (9) is periodic in 3-dimensional coordinate system, it can be numerically solved by the Fast Fourier Transform and SPM for zeroth-order, first-order, or higher-order approximation.

Zeroth-order approximation: By assuming the relative permeability to be homogeneous (namely $\Delta\mu_{ij}(\mathbf{r})$ is zero) and solving Eq. (9), we have

$$\mu_{ij}^0 \frac{\partial^2 \varphi_m^0(\mathbf{r})}{\partial x_i \partial x_j} = \frac{\partial M_i^S(\mathbf{r})}{\partial x_i}. \quad (10)$$

This equation can be solved in Fourier space

$$-\mu_{ij}^0 q_i q_j \tilde{\varphi}_m^0(\mathbf{q}) = I q_i \tilde{M}_i^S(\mathbf{q}), \quad (11)$$

where $\tilde{\varphi}_m^0(\mathbf{q})$ and $\tilde{M}_i^S(\mathbf{q})$ are Fourier transforms of $\varphi_m^0(\mathbf{r})$ and $M_i^S(\mathbf{r})$, $\tilde{\varphi}_m^0(\mathbf{q}) = \int_V \varphi_m^0(\mathbf{r}) e^{-i\mathbf{q}\cdot\mathbf{r}} d^3r$, $\tilde{M}_i^S(\mathbf{q}) = \int_V M_i^S(\mathbf{r}) e^{-i\mathbf{q}\cdot\mathbf{r}} d^3r$, respectively, \mathbf{q} is the reciprocal lattice vector, q_j is the j th component of \mathbf{q} , and I is the imaginary unit, then we get

$$\tilde{\varphi}_m^0(\mathbf{q}) = -I q_i G(\mathbf{q}) \tilde{M}_i^S(\mathbf{q}), \quad (12)$$

where $G^{-1}(\mathbf{q}) = \mu_{ij}^0 q_i q_j$. After inverse Fourier transforms on both sides of Eq. (12), we obtain the zeroth-order approximation of the demagnetization potential,

$$\varphi_m^0(\mathbf{r}) = - \int \frac{d^3q}{(2\pi)^3} I q_i G(\mathbf{q}) \tilde{M}_i^S(\mathbf{q}) e^{i\mathbf{q}\cdot\mathbf{r}}. \quad (13)$$

Using Fourier transformation method to solve $H_j^{d-0}(\mathbf{r}) = -\nabla_j \varphi_m^0(\mathbf{r})$, we can obtain the zeroth-order demagnetization field

$$H_j^{d-0}(\mathbf{r}) = - \int \frac{d^3q}{(2\pi)^3} I q_j \tilde{\varphi}_m^0(\mathbf{q}) e^{i\mathbf{q}\cdot\mathbf{r}}. \quad (14)$$

First-order approximation: Substituting the zeroth-order demagnetization potential Eq. (13) and demagnetization field Eq. (14) in the iterative Eq. (9), we can obtain the first-order demagnetization potential iteration

$$\mu_{ij}^0 \frac{\partial^2 \varphi_m^1(\mathbf{r})}{\partial x_i \partial x_j} = \frac{\partial}{\partial x_i} \left[\Delta \mu_{ij}(\mathbf{r}) \left(H_j^{\text{ext}} + H_j^{d-0}(\mathbf{r}) \right) + M_i^S(\mathbf{r}) \right]. \quad (15)$$

The solution of $\varphi_m^1(\mathbf{r})$ is obtained in Fourier space

$$\tilde{\varphi}_m^1(\mathbf{q}) = -I q_i G(\mathbf{q}) \left\{ \Delta \mu_{ij}(\mathbf{r}) \left(H_j^{\text{ext}} + H_j^{d-0}(\mathbf{r}) \right) + M_i^S(\mathbf{r}) \right\}_{\mathbf{q}}, \quad (16)$$

where $\left\{ \Delta \mu_{ij}(\mathbf{r}) \left(H_j^{\text{ext}} + H_j^{d-0}(\mathbf{r}) \right) + M_i^S(\mathbf{r}) \right\}_{\mathbf{q}}$ indicates the Fourier transforms of $\Delta \mu_{ij}(\mathbf{r}) \left(H_j^{\text{ext}} + H_j^{d-0}(\mathbf{r}) \right)$, and the first-order demagnetization field can be obtained by

$$H_j^{d-1}(\mathbf{r}) = - \int \frac{d^3q}{(2\pi)^3} I q_j \tilde{\varphi}_m^1(\mathbf{q}) e^{i\mathbf{q}\cdot\mathbf{r}}. \quad (17)$$

Higher-order approximation: The higher-order solutions for $\varphi_m(\mathbf{r})$ are derived in a similar way as the first-order approximation

$$\mu_{ij}^0 \frac{\partial^2 \varphi_m^n(\mathbf{r})}{\partial x_i \partial x_j} = \frac{\partial}{\partial x_i} \left[\Delta \mu_{ij}(\mathbf{r}) \left(H_j^{\text{ext}} + H_j^{d-(n-1)}(\mathbf{r}) \right) + M_i^S(\mathbf{r}) \right]. \quad (18)$$

Similar as $\varphi_m^1(\mathbf{r})$, the solution for $\varphi_m^n(\mathbf{r})$ is solved using Fourier transforms

$$\tilde{\varphi}_m^n(\mathbf{q}) = -I q_i G(\mathbf{q}) \left\{ \Delta \mu_{ij}(\mathbf{r}) \left(H_j^{\text{ext}} + H_j^{d-(n-1)}(\mathbf{r}) \right) + M_i^S(\mathbf{r}) \right\}_{\mathbf{q}}, \quad (19)$$

and the higher-order demagnetization field can be obtained by

$$H_j^{d-n}(\mathbf{r}) = - \int \frac{d^3q}{(2\pi)^3} I q_j \tilde{\varphi}_m^n(\mathbf{q}) e^{i\mathbf{q}\cdot\mathbf{r}}. \quad (20)$$

As for the total magnetic scalar potential $\Phi_m(\mathbf{r})$, with given boundary conditions, it can be solved from

$$H_j^{\text{ext}} + H_j^d(\mathbf{r}) = -\nabla_j \Phi_m(\mathbf{r}). \quad (21)$$

Once the magnetic field distribution is obtained, the total magnetization can be calculated from Eq. (1),

$$M_i(\mathbf{r}, \mathbf{H}) = M_i^S(\mathbf{r}) + \chi_{ij}^m(\mathbf{r}) H_j(\mathbf{r}). \quad (22)$$

The effective magnetic susceptibility tensor χ_{ij}^{eff} of the composite can be determined from Eq. (22) by solving

$$\langle M_i(\mathbf{r}, \mathbf{H}) - M_i^S(\mathbf{r}) \rangle = \chi_{ij}^{\text{eff}} \langle H_j(\mathbf{r}) \rangle. \quad (23)$$

III. RESULT AND DISCUSSION

For checking the accuracy of the proposed SPM, we first employed two static magnetic inhomogeneous systems as examples to perform the 3-dimensional simulations: a ferromagnetic sphere in infinite vacuum and a ferromagnetic hollow ball in a homogeneous magnetic field. Then, we studied the effective magnetic susceptibility and local magnetic field distribution in a two-phase magnetic composite with different inclusion characteristics.

A. A ferromagnetic sphere in infinite vacuum

In the example of an isolated ferromagnetic sphere in vacuum, as shown in Figure 1(a), the radius of the ferromagnetic sphere is taken to be much smaller than the simulation size for decreasing the overlapping effect on the solutions induced by the periodic boundary conditions. A grid size of $128 \times 128 \times 128$ is used for the simulation, and the radius (R_0) of the ferromagnetic sphere is assigned a value of 16. A spontaneous magnetization of $M^S = 10^6$ A/m along x -direction and an isotropic magnetic susceptibility of 100 are assumed for the ferromagnetic sphere. To alleviate the Gibbs effect in Fourier transforms in the spectral method arising from a sharp interface, a diffuse-interface shape function to describe the vacuum and the ferromagnetic is introduced as the following:

$$\eta(\mathbf{r}) = \frac{1}{2} \left\{ 1.0 - \tanh[\gamma(d(\mathbf{r}) - R_0)] \right\}, \quad (24)$$

where $d(\mathbf{r})$ is the distance of any point (x, y) from the center of the sphere, and γ is a positive parameter controlling the width of the surface. As a result, η has a value of 1 inside the ball and a value of 0 outside of the ball.

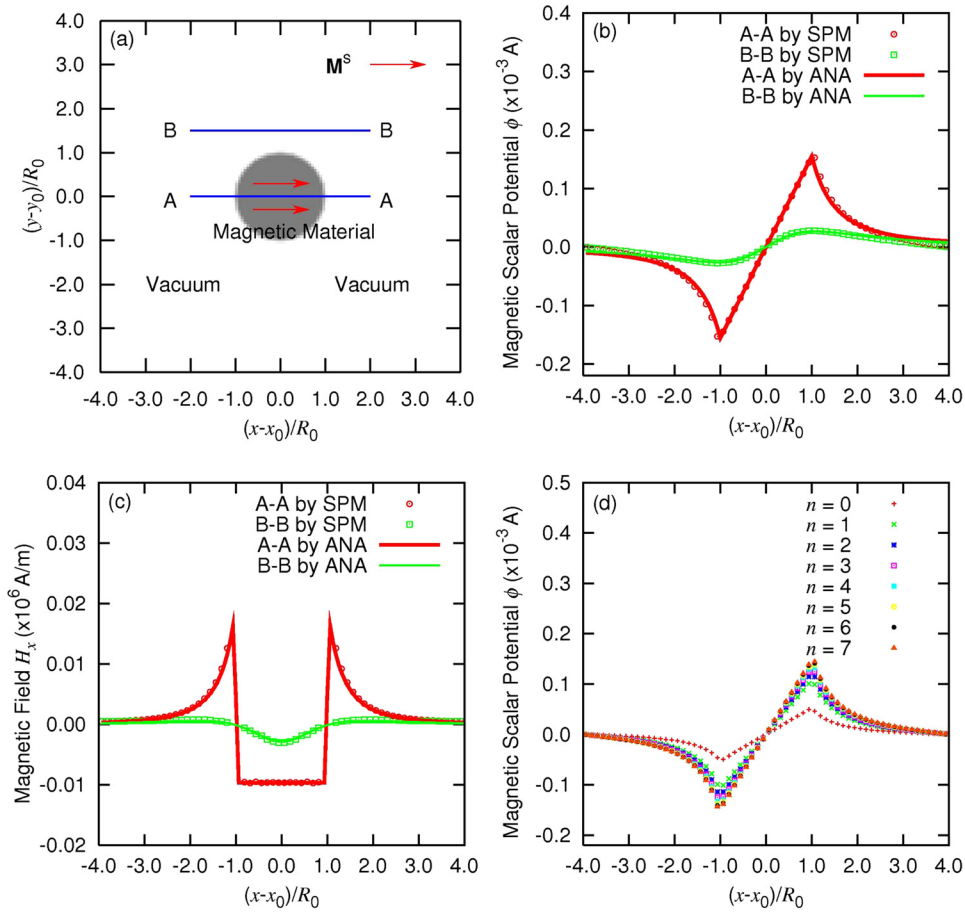


FIG. 1. (a) Schematics of the middle section (parallel to x - y plane) of an isolated ferromagnetic sphere with self-polarization \mathbf{M}^S along x direction surrounded by vacuum, where R_0 indicates the radius of the sphere. (b) Magnetic scalar potential ϕ along A-A and B-B cross-sections calculated from SPM comparing with analytical expression. (c) Local magnetic field component H_x along A-A and B-B cross-sections calculated from SPM comparing with analytical expression. (d) Solution of the magnetic scalar potential ϕ along A-A cross-section as a function of iteration numbers from SPM.

The analytical solution of the static magnetic equilibrium equation for such a special case obtained by solving the Laplace equation with boundary conditions is as follows:

$$\varphi(\mathbf{r}) = \begin{cases} \frac{\mathbf{M} \cdot \mathbf{r}}{3}, & (r \leq R_0) \\ \frac{R_0^3 \mathbf{M} \cdot \mathbf{r}}{3r^3}, & (r > R_0), \end{cases} \quad (25)$$

where \mathbf{M} is the total magnetization and $r = \sqrt{x^2 + y^2 + z^2}$. Note that the total magnetization \mathbf{M} in Eq. (25) is not same as the spontaneous magnetization \mathbf{M}^S in Eq. (1) because \mathbf{M} is the result of considering the induced magnetization due to the demagnetization field in the ferromagnetic sphere, and they correlate with each other by $\mathbf{M} = 3\mathbf{M}^S/(\chi + 3)$ for this special case. It can be seen from Figures 1(b) and 1(c) that the numerical solutions of the magnetic scalar potential and magnetic field agree well with the analytical results through the whole cross sections of both A-A and B-B, except a slight discrepancies at the boundary and interface. The difference between the numerical solution and the analytical solution stems from the fact that the numerical solutions are obtained with periodic boundary conditions with a diffuse-interface description for the sphere surface while the analytical solution is for ideal sphere in an infinite matrix with a sharp-interface description. Also, the solution shows that the local magnetic field is homogeneous inside the sphere. The local magnetic field

has maximal values on the interface along A-A cross section, and it decreases gradually to zero in the vacuum far away from the ferromagnetic particle.

Since each order of the approximation for the magnetic solution is obtained analytically (see Eqs. (15) and (18)), the proposed algorithm is extremely efficient. Figure 3(d) shows solutions of the magnetic scalar potential along A-A cross section with iterative numbers. As one can see, the solutions converge very fast, and a third-order solution can reach a very good approximation for this special case.

B. A magnetic hollow ball in an external homogeneous magnetic field

In the second example, the magnetic scalar potential and magnetic field distribution of a hollow ball with zero spontaneous magnetization in an external homogeneous magnetic field are calculated using the proposed SPM and compared with the analytical results. As shown in Figure 2(a), the inner radius R_1 and outer radius R_2 of the hollow ball are assigned values of 16 and 24. Similar as Eq. (25), Eq. (26) is the shape function of the hollow ball for distinguishing the vacuum and the ferromagnetics

$$\eta(\mathbf{r}) = \frac{1}{2} \{ \tanh[\gamma(d(\mathbf{r}) - R_1)] - \tanh[\gamma(d(\mathbf{r}) - R_2)] \}. \quad (26)$$

The analytical solution of the static magnetic equilibrium equation for this case is as follows:

$$\phi(\mathbf{r}) = \begin{cases} -9(\chi + 1)(\mathbf{H}^{\text{ext}} \cdot \mathbf{r})/K, & (r \leq R_1) \\ -3(2\chi + 3)(\mathbf{H}^{\text{ext}} \cdot \mathbf{r})/K - 3\chi R_1^3(\mathbf{H}^{\text{ext}} \cdot \mathbf{r})/(Kr^3), & (R_1 < r \leq R_2) \\ -\mathbf{H}^{\text{ext}} \cdot \mathbf{r} + \chi(2\chi + 3)(R_2^3 - R_1^3)(\mathbf{H}^{\text{ext}} \cdot \mathbf{r})/(Kr^3), & (r > R_2), \end{cases} \quad (27)$$

where $r = \sqrt{x^2 + y^2 + z^2}$ and $K = (2\chi + 3)(\chi + 3) - 2\chi^2 (R_1/R_2)^3$. We consider two magnetic hollow balls with magnetic susceptibility equal to 5 and 50, respectively, to study the magnetic shielding effect. It can be seen from Figures 2(b) and 2(c) that the numerical solutions of the magnetic scalar potential and magnetic field agree well with the analytical results through the whole cross sections of both A-A and B-B for both the two cases. The magnetic field is discontinuous along A-A cross section: In the center-hole area, it is homogeneous and jumps at the inner interface, while at the outer interface, it jumps again to the maximal value and then decreases to external magnetic field in vacuum far away from the interface. The discontinuity of the magnetic field is shown more clearly by Figure 2(d). With the magnetic susceptibility increasing from 5 to 50, it can be seen from Figure 2(c) that the magnetic field inside the magnetic gets much closer to zero, which means that the center-hole area is shielded from the external magnetic field. With the magnetic susceptibility of the magnetic hollow ball becoming larger, this shielding is more obvious, and the magnetic field at the outer interface becomes larger.

C. A two-phase composite with different microstructures

The formulated SPM in Sec. II is employed to study the effects of the microstructure on the effective magnetic susceptibility and magnetic field concentration of a two-phase composite. As the microstructure is associated with many factors such as the size, shape, volume fraction, spatial arrangement of inclusion particles, and the magnetic susceptibility mismatch between the inclusion and matrix, and so on. Due to that, most of the factors have been investigated by the phase field method in the work of Wang *et al.* on the dielectric composite,²⁷ which is similar as the magnetic composite system; here, therefore, we only focus on: the magnetic susceptibility mismatch between the inclusion and matrix, inclusion volume fraction, and spatial arrangement. Although the SPM is formulated in general 3-dimensional situation, 2-dimensional computations are performed here to make affordable the large amount of computations as required for this work, and the above two examples have already verified that the proposed SPM works for 3-dimensional cases. Additionally, we assume that the

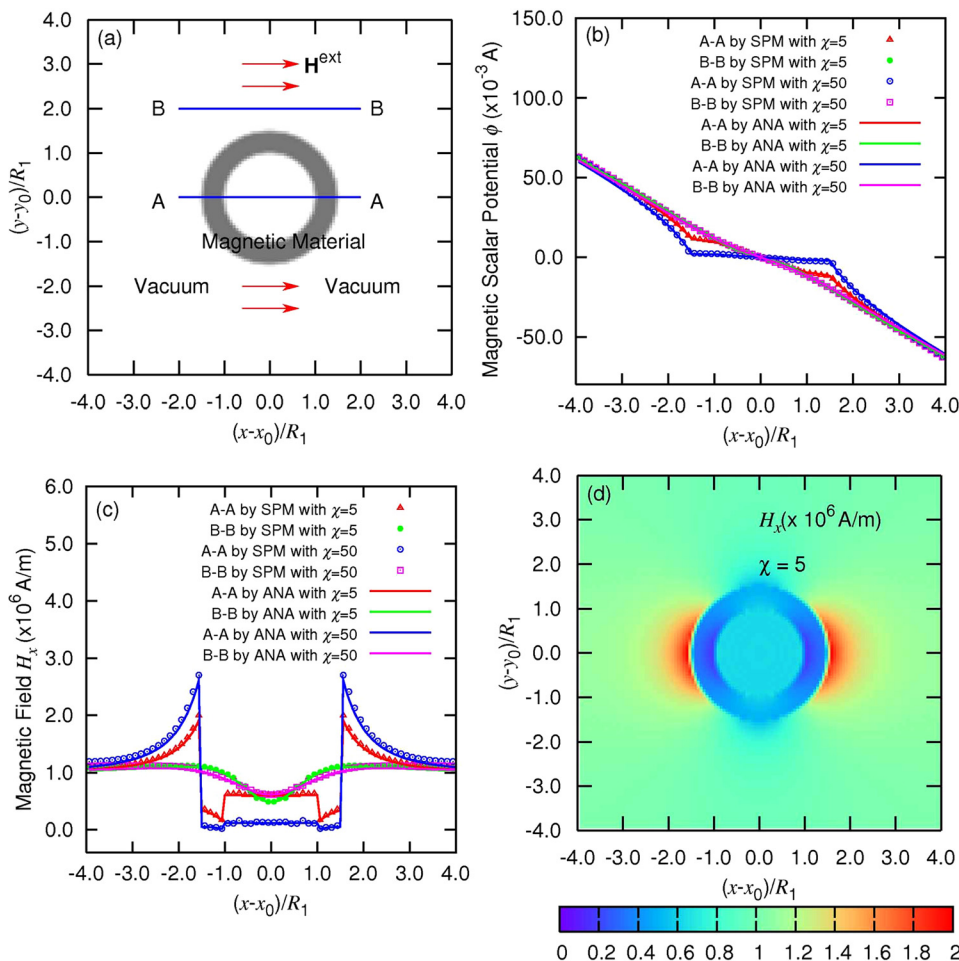


FIG. 2. (a) Schematics of the middle section (parallel to x-y plane) of an isolated magnetic hollow ball in a homogeneous external magnetic field \mathbf{H}^{ext} , where R_1 and R_2 indicate the inner and outer radius of the hollow ball, respectively. For two magnetics with different susceptibility. (b) Magnetic scalar potential ϕ along A-A and B-B cross-sections calculated from SPM comparing with analytical expression. (c) Local magnetic field component H_x along A-A and B-B cross-sections calculated from SPM comparing with analytical expression. (d) Contour for the solution of the magnetic scalar potential ϕ of the middle-section for a magnetic with susceptibility $\chi = 5$.

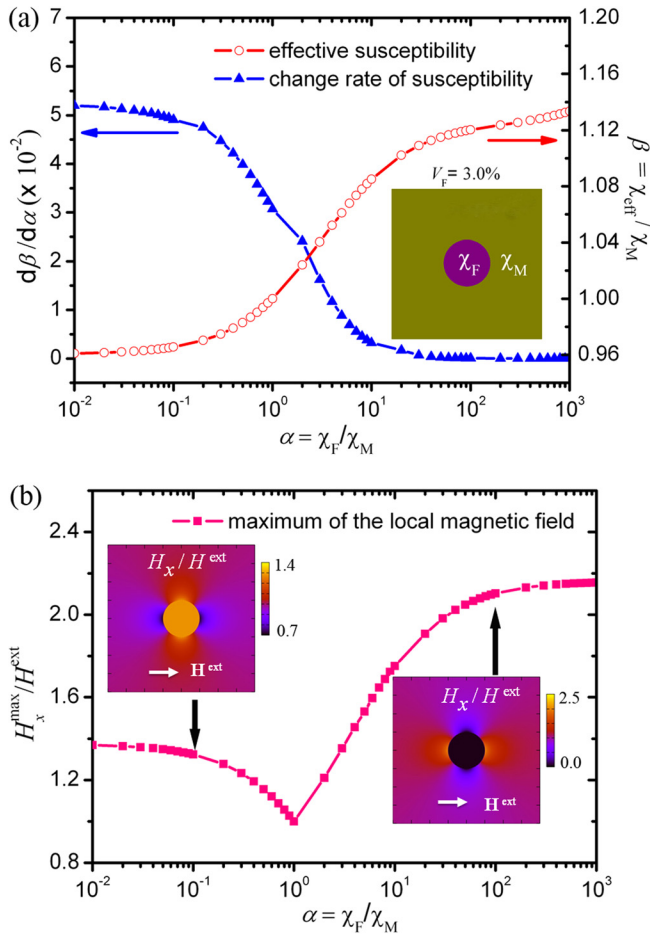


FIG. 3. For a two-phase composite with single inclusion particle at a volume fraction of 3.0%, effects of the susceptibility mismatch on (a) the effective susceptibility and (b) the distribution of component H_x of the maximal local magnetic field. The variables of χ_F and χ_M indicate the isotropic magnetic susceptibilities of the inclusion particle and matrix, respectively.

magnetic susceptibility of the inclusion and matrix are isotropic for simplification, although the proposed SPM is formulated for composites with arbitrary anisotropy, and we use χ_F and χ_M to indicate the isotropic magnetic susceptibilities of the inclusion and matrix, respectively.

We first investigate effects of the magnetic susceptibility mismatch between the inclusion and matrix on the effective magnetic susceptibility and local magnetic field distribution in a two-phase composite with single inclusion particle at a volume fraction 3.0%, as shown in Figures 3(a) and 3(b). Two variables are introduced to describe the magnetic

susceptibility mismatch effect on the effective susceptibility of the composite: One is $\alpha = \chi_F/\chi_M$ named susceptibility mismatch ratio of the inclusion to the matrix, and the other is $\beta = \chi_{\text{eff}}/\chi_M$ named effective susceptibility ratio of the composite to the matrix. In this work, the susceptibility χ_M of the matrix is kept constant, and the susceptibility χ_F of the inclusion is adjusted to change the susceptibility mismatch ratio α . It can be seen from Figure 3(a) that with the increase in α , β increases, while $d\beta/d\alpha$ decreases. The effective susceptibility is getting close to saturation when the susceptibility mismatch ratio is about 50, which is similar as the result of dielectric composite system from the phase field simulation.²⁷ With regard to the local magnetic field concentration, it can be seen from Figure 3(b) that the magnitude of maximal local magnetic field component $H_x^{\max}/H^{\text{ext}}$ decreases when $\alpha \leq 1$ and increases when $\alpha > 1$ with α increasing. Therefore, it can be concluded that the susceptibility mismatch can introduce the local magnetic field concentration. The two insets in Figure 3(b) exhibit the distribution of the local magnetic field component H_x/H^{ext} when $\alpha = 10^{-1}$ and $\alpha = 10^2$, respectively. It can be seen that the magnetic field inside the inclusion is homogeneous which is strengthened when $\alpha < 1$ but weakened when $\alpha > 1$.

In order to investigate the effect of the inclusion volume fraction on the effective susceptibility, the proposed SPM and some phenomenological approximations are used to calculate the effective susceptibility and make comparison. The predication of the effective susceptibility from the MG equation is described by

$$\chi_{\text{eff}} = \chi_M + \frac{dV_F\lambda\chi_M}{1 - V_F\lambda}, \quad (28)$$

where d is the dimensionality of the system and $\lambda = (\chi_F - \chi_M)/(\chi_F + (d-1)\chi_M)$. In the BH equation, the effective susceptibility is indirect and has to be solved, as shown in the following equation:

$$\frac{\chi_{\text{eff}} - \chi_F}{\chi_M - \chi_F} \left(\frac{\chi_M}{\chi_{\text{eff}}} \right)^{1/3} = 1 - V_F. \quad (29)$$

For Looyenga equation, it is, in fact, a special case with $n = 1/3$ in the Lichtenecker-Rother mixing rule

$$(\chi_{\text{eff}})^n = [(1 - V_F)(\chi_M)^n + V_F(\chi_F)^n]. \quad (30)$$

The Meredith-Tobias equation is more rigorous equation with higher order of V_F based on the Maxwell-Garnett model

$$\frac{\chi_{\text{eff}}}{\chi_M} = 1 + \frac{3V_F\lambda - 4.221\lambda(V_F)^{10/3}(\chi_F - \chi_M)/(3\chi_F + 4\chi_M)}{1 - V_F\lambda - \lambda \left(1.227(V_F)^{7/3} + 2.178(V_F)^{10/3} \right) (\chi_F - \chi_M)/(3\chi_F + 4\chi_M)}, \quad (31)$$

where λ has the same meaning in Eq. (28). Two cases are considered here to calculate the corresponding effective susceptibility and local field distribution. The first case is a

two-phase composite with a single inclusion particle but different inclusion particles volume fraction due to the different size. In this case, there is no interaction among inclusion

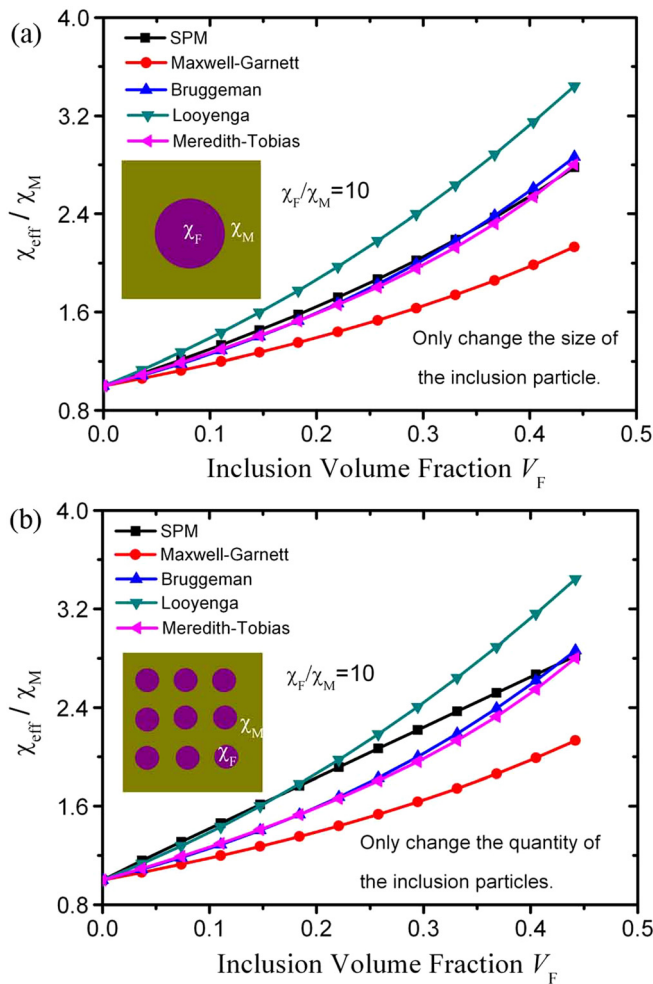


FIG. 4. Effects of inclusion volume fraction on the effective susceptibility of a two-phase composite with (a) single and (b) multi inclusion particles, respectively. The black line with square in (a) and (b) indicates the numerical results calculated from the proposed SPM method, compared with analytical results calculated from other phenomenological approximations. The variables of χ_F and χ_M indicate the isotropic magnetic susceptibilities of the inclusion particle and the matrix, respectively, and χ_{eff} indicates the effective magnetic susceptibility of the composite.

particles except the overlapping effect induced by the periodic boundary condition. It can be seen from Figure 4(a) that the proposed SPM, Bruggeman approximation, and Meredith-Tobias approximation give very close results for the single inclusion particle case. As for the Maxwell-Garnett approximation, it underestimates the effective susceptibility especially when the volume fraction of the inclusion particle is high. On the contrary, the Looyenga approximation overestimates the effective susceptibility especially when the volume fraction of the inclusion particle is high. The second case is also a two-phase composite but with multi inclusion particles, and the volume fraction of the inclusion particles can be changed by adjusting the quantity. In this case, there are interactions among inclusion particles besides the periodic boundary condition induced overlapping effect. For this case, as shown in Figure 4(b), the proposed SPM and Looyenga approximation give the closest results for the effective susceptibility when the volume fraction of the inclusion particle is lower than 20%. However, when the

inclusion volume fraction is higher than 20%, the Looyenga model gives higher result of the effective susceptibility than the SPM. In other words, The Looyenga model is a good approximation when the inclusion particle dispersion is moderately sparse. Similar as the first case, the Maxwell-Garnett model always underestimate the effective susceptibility compared with all other approximations. However, for this multi inclusions case, the Bruggeman and Meredith-Tobias approximations also underestimate the effective susceptibility compared to the proposed SPM when the volume fraction of the inclusion particle is lower than 44%, and it seems that this tendency is broken at $V_F = 44\%$ beyond which the results from Bruggeman and Meredith-Tobias approximations will be higher than from SPM.

The spatial arrangement of inclusion particles is also an important factor in determining the effective susceptibility and local magnetic field concentration. For example, it has been shown in experiments that the effective susceptibility and breakdown strength (for dielectric composites) can be greatly affected by the alignments of the inclusion particles.^{28–31} In this work, two different structures, an isotropic structure with well-dispersed inclusion particles and an anisotropic structure with chain-dispersed inclusion particles, are used to study the effects of the susceptibility mismatch on the effective susceptibility and local magnetic field concentration. Figure 5(a) shows the effective susceptibility affected by the susceptibility mismatch for a two-phase composite with two different inclusion particles arrangements. For the isotropic structure with well-dispersed inclusion particles, the effective susceptibility is also isotropic with the assumption that the susceptibilities of the inclusion particles and matrix are isotropic. While for the anisotropic structure with chain-dispersed inclusion particles, the effective susceptibility becomes anisotropic although the susceptibilities of the inclusion particles and matrix are isotropic. With the susceptibility mismatch ratio α increasing, the effective susceptibility component in x direction for the chain-structured composite increases greatly faster than the component along y direction and the isotropic counterpart. Additionally, the effective susceptibility component in y direction is always smaller than the isotropic case. As for the reason, it can be attributed to the demagnetization effects induced by the interfaces in the composite. For composite with well-dispersed inclusion particles at volume fraction $V_F = 19.6\%$, the interactions between particles are not strong enough to significantly reduce the demagnetization effect of individual particles; thus, the composites exhibit moderate effective susceptibility in all directions. However, with particles aligned into chains, particles strongly interact through static magnetic forces in the chain direction to greatly reduce the demagnetization effect of the particles in each chain, resulting in significantly improved effective susceptibility along the chain direction. In the transverse direction, on the other hand, the strong chain-chain interactions enhance the demagnetization effect, leading to the decreased effective susceptibility component. Therefore, the chain-structured composites exhibit significant effective susceptibility anisotropy, which results from the microstructure anisotropy of the inclusion particles arrangement.

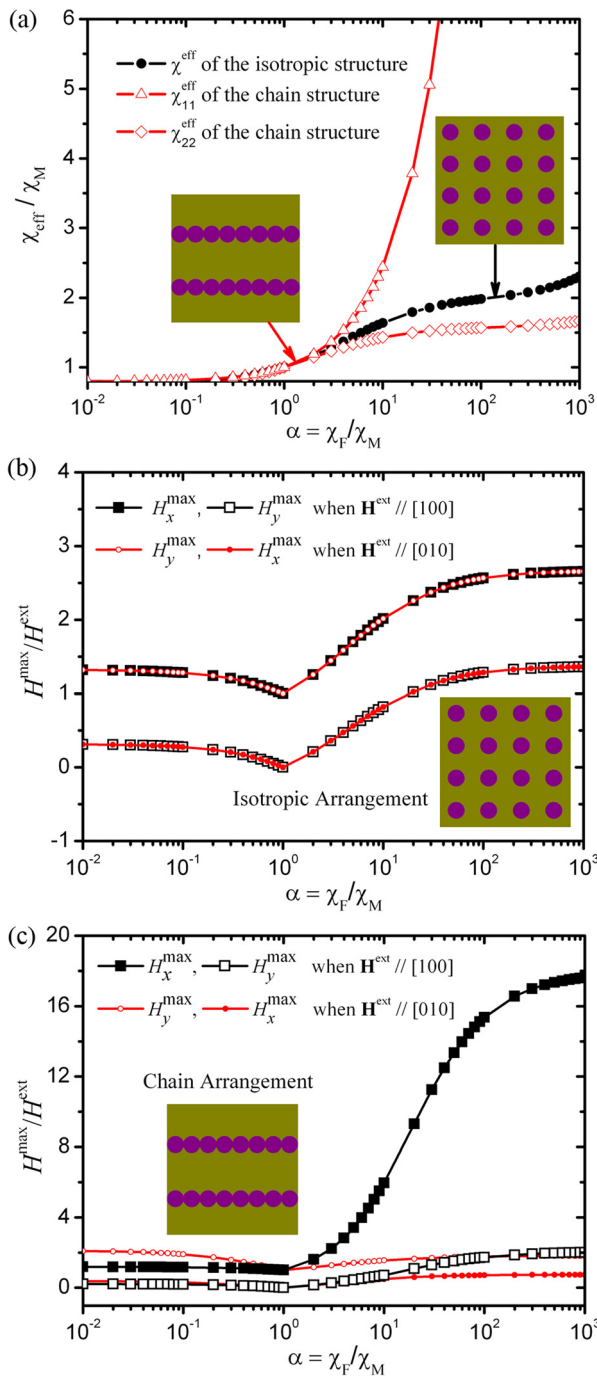


FIG. 5. Effect of the arrangement of the inclusion particles on (a) the effective susceptibility and (b) and (c) the local magnetic field concentration of a two-phase composite with multi inclusion particles. Both the inclusion particles volume fractions in these two structures are $V_F = 19.6\%$, and externally applied magnetic fields along [100] and [010] directions are used to calculate the local field distribution. The susceptibility mismatch ratio are taken $\alpha = 10$. The variables of χ_F and χ_M indicate the isotropic magnetic susceptibilities of the inclusion particle and the matrix, respectively, and χ_{eff} indicates the effective magnetic susceptibility of the composite.

Not only the effective susceptibility, but also can the local magnetic field contribution be significantly affected by the inclusion particles arrangement. As shown in Figure 5(b), the maximal magnitude of the local magnetic field as function of the susceptibility mismatch ratio α for the composite with isotropic arrangement of the inclusion particles

are calculated when the external magnetic field \mathbf{H}^{ext} are applied along x (namely [100]) and y (namely [010]) directions, respectively. It can be seen that whatever the external magnetic field is along [100] or [010] direction, the maximal local magnetic fields along the \mathbf{H}^{ext} direction (see the black line with solid squares and the red line with open circles) are the same and higher than the transverse counterparts (see the black line with open squares and the red line with solid circles), indicating an isotropic characteristic. However, for the composite with chain arrangement of the inclusion particles, as shown in Figure 5(c), the maximal magnitude of the local magnetic field H_x^{max} when \mathbf{H}^{ext} is along [100] direction (see the black line with solid squares) is greatly higher than H_y^{max} when \mathbf{H}^{ext} is along [010] direction (see the red line with open circles), exhibiting a huge anisotropy.

Figures 6(a)–6(f) give the local distributions of the magnetic field in those two kinds of composites when the externally applied magnetic field is along [100] and [010] directions. For the composite with isotropic inclusion particles arrangement, the magnetic field distributions under x-direction external magnetic field and y-direction external magnetic field can be equivalent by transforming the coordinates; thus, we only showed the case under x-direction external magnetic field. It can be seen from Figures 6(a)–6(f) that the local magnetic field concentrates severely in the matrix region near the particles. For the parallel component of the local magnetic field, it concentrates along the direction of the external magnetic field. For the perpendicular component of the local magnetic field, it concentrates along a direction

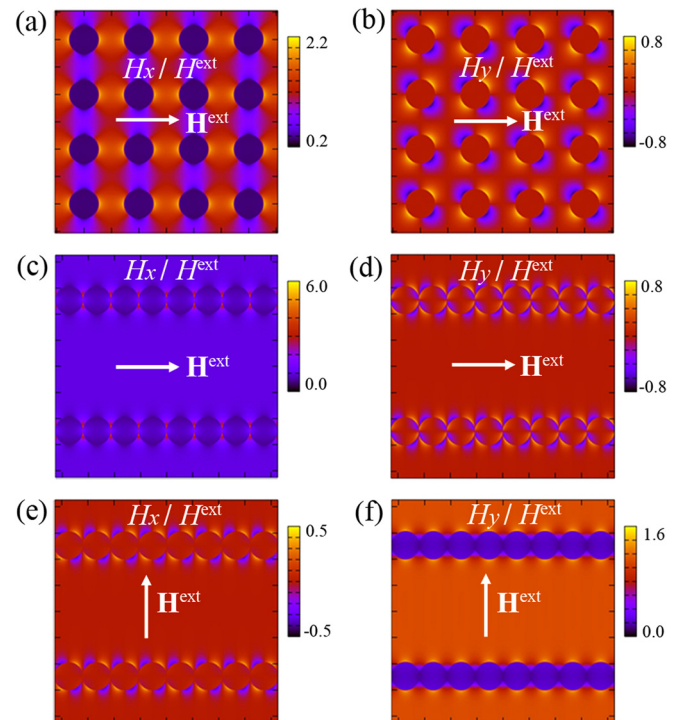


FIG. 6. The local magnetic field distributions of a two-phase composite with the susceptibility mismatch ratio $\alpha = 10$ and inclusion particles volume fraction $V_F = 19.6\%$ for two different inclusion particles arrangements, i.e., an isotropic dispersion and a chain-structured dispersion of the inclusion particles, under externally applied magnetic field along [100] and [010], respectively.

which forms a 45° or 135° angle with the direction of the externally applied magnetic field. In the anisotropic structure with chain-arranged inclusion particles, the concentration for the normal component of the local magnetic field is much more serious than the isotropic case. In such an anisotropic structure, the close connectivity of the inclusion particles along the chain direction and greatly reduced demagnetization factor allow the magnetic field to penetrate into the inclusion particles and propagate through the chains, leading to a high effective susceptibility while, on the other hand, concentrating the large local magnetic field in the matrix at the necks and gaps between particles. Although the local electric field concentration in dielectric composites is harmful to the breakdown strength of high density energy-storage materials, the local magnetic field concentration in magnetic composite can be pretty useful to improve the sensitivity of magnetic sensors and promote the development of magnetic nano-particles for gene and drug delivery.^{32,33} Therefore, both the effective susceptibility and local magnetic field concentration are affected by the microstructure of the magnetic composite, and how to utilize the improvement of the effective susceptibility and the local magnetic field concentration lies on the actual requirements.

IV. CONCLUSION

In summary, an efficient algorithm based on the proposed Fourier spectral iterative perturbation method is used to compute properties of the magnetic composite with arbitrary susceptibility inhomogeneity and anisotropy. The accuracy of the proposed method is studied by comparing the numerical results with analytical results, and the comparisons show good agreements, validating that the proposed algorithm is an accurate tool for predicting the effective properties of the magnetic composite, especially when the interactions between inclusion particles are strong. The effects of the microstructures including the susceptibility mismatch between the inclusion particles and matrix, inclusion particles volume fraction, and inclusion particles arrangement on the magnetic composite are investigated. It is concluded that the static magnetic interactions among the inclusion particles embedded in the matrix play critical roles in determining the composite properties, which sensitively depend on inclusion particles arrangement and, especially, the chain structure. Such chain structure exhibits strong effective susceptibility anisotropy despite all constituent components being isotropic. The proposed method is a good tool to design a composite with appropriate microstructures for pursuing simultaneously the improvement of the effective susceptibility and concentration of the local magnetic

field. The studies in this work not only work for the magnetic composite but also for the dielectric composite.

ACKNOWLEDGMENTS

This work was supported by the NSF of China (Grant Nos. 11234005, 51332001, 51221291, and 51472140), and the NSF (Grant Nos. DMR-1410714, DMR-0820404, and DMR-1210588).

- ¹D. R. Smith, W. J. Padilla, D. C. Vier, S. C. Nemat-Nasser, and S. Schultz, *Phys. Rev. Lett.* **84**, 4184 (2000).
- ²Y. S. Lin, S. H. Wu, Y. Hung, Y. H. Chou, C. Chang, M. L. Lin, C. P. Tsai, and C. Y. Mou, *Chem. Mater.* **18**, 5170 (2006).
- ³H. Shokrollahi and K. Janghorban, *J. Mater. Process. Technol.* **189**, 1 (2007).
- ⁴C. W. Nan, M. I. Bichurin, S. X. Dong, D. Viehland, and G. Srinivasan, *J. Appl. Phys.* **103**, 031101 (2008).
- ⁵R. F. Gibson, *Compos. Struct.* **92**, 2793 (2010).
- ⁶L. Sandlund, M. Fahlander, T. Cedell, A. E. Clark, J. B. Restorff, and M. Wun-Fogle, *J. Appl. Phys.* **75**, 5656 (1994).
- ⁷J. M. Ginder, M. E. Nichols, L. D. Elie, and S. M. Clark, *Int. Soc. Opt. Eng.* **3985**, 418 (2000).
- ⁸J. C. M. Garnett, *Philos. Trans. R. Soc., A* **203**, 385 (1904).
- ⁹R. Landauer, *AIP Conf Proc.* **40**, 2 (1978).
- ¹⁰D. A. G. Bruggeman, *Ann. Phys.* **416**, 636 (1935).
- ¹¹T. Hanai, Bulletin of the Institute for Chemical Research, Kyoto University **39**, 341 (1962), available online at <http://hdl.handle.net/2433/75873>.
- ¹²P. Sen, C. Scala, and M. Cohen, *Geophysics* **46**, 781 (1981).
- ¹³H. Looyenga, *Physica* **31**, 401 (1965).
- ¹⁴Z. Hashin and S. Shtrikman, *J. Appl. Phys.* **33**, 3125 (1962).
- ¹⁵R. E. Meredith and C. W. Tobias, *J. Appl. Phys.* **31**, 1270 (1960).
- ¹⁶L. Fu, P. B. Macedo, and L. Resca, *Phys. Rev. B* **47**, 13818 (1993).
- ¹⁷Y. Pittini-Yamada, E. A. Perigo, Y. de Hazan, and S. Nakahara, *Acta Mater.* **59**, 4291 (2011).
- ¹⁸Y. U. Wang, *Appl. Phys. Lett.* **96**, 232901 (2010).
- ¹⁹Y. U. Wang, Y. M. Jin, and A. G. Khachatryan, *Appl. Phys. Lett.* **80**, 4513 (2002).
- ²⁰Y. U. Wang, Y. M. Jin, and A. G. Khachatryan, *J. Appl. Phys.* **92**, 1351 (2002).
- ²¹J. J. Wang, S. Bhattacharyya, Q. Li, T. W. Heo, X. Q. Ma, and L. Q. Chen, *Philos. Mag. Lett.* **92**, 327 (2012).
- ²²S. Y. Hu and L. Q. Chen, *Acta Mater.* **49**, 1879 (2001).
- ²³P. Yu, S. Y. Hu, L. Q. Chen, and Q. Du, *J. Comput. Phys.* **208**, 34 (2005).
- ²⁴T. W. Heo, S. Bhattacharyya, and L. Q. Chen, *Acta Mater.* **59**, 7800 (2011).
- ²⁵S. Bhattacharyya, T. W. Heo, K. Chang, and L. Q. Chen, *Commun. Comput. Phys.* **11**, 726 (2012).
- ²⁶J. J. Wang, X. Q. Ma, Q. Li, J. Britson, and L. Q. Chen, *Acta Mater.* **61**, 7591 (2013).
- ²⁷Y. U. Wang and D. Q. Tan, *J. Appl. Phys.* **109**, 104102 (2011).
- ²⁸V. Tomer, C. A. Randall, G. Polizos, J. Kostelnick, and E. Manias, *J. Appl. Phys.* **103**, 034115 (2008).
- ²⁹V. Tomer and C. A. Randall, *J. Appl. Phys.* **104**, 074106 (2008).
- ³⁰Y. Song, Y. Shen, H. Y. Liu, Y. H. Lin, M. Li, and C. W. Nan, *J. Mater. Chem.* **22**, 16491 (2012).
- ³¹P. H. Hu, J. J. Wang, Y. Shen, Y. H. Guan, Y. H. Lin, and C. W. Nan, *J. Mater. Chem. A* **1**, 12321 (2013).
- ³²O. Veisoh, J. W. Gunn, and M. Zhang, *Adv. Drug Deliver Rev.* **62**, 284 (2010).
- ³³J. Dobson, *Nanomedicine* **1**, 31 (2006).